Makara Journal of Technology

Volume 23 | Issue 3 Article 1

12-3-2019

Comprehensive Inspection on the Experimental Ferritic Stainless Steel by Means of Transmission Electron Microscopy and Neutron Diffraction Techniques

Parikin Parikin
Science and Technology of Advanced Materials, National Nuclear Energy Agency (BATAN), South Tangerang 15314, Indonesia, farihin@batan.go.id

Mohammad Dani
Science and Technology of Advanced Materials, National Nuclear Energy Agency (BATAN), South Tangerang 15314, Indonesia

Riza Iskandar
Central Facility for Electron Microscopy (GFE), RWTH Aachen University, Ahornstrasse.55, D-52074 Aachen, Germany

Aziz Khan Jahja
Science and Technology of Advanced Materials, National Nuclear Energy Agency (BATAN), South Tangerang 15314, Indonesia

Andon Insani
Science and Technology of Advanced Materials, National Nuclear Energy Agency (BATAN), South Tangerang 15314, Indonesia

Follow this and additional works at: https://scholarhub.ui.ac.id/mjt

Part of the Chemical Engineering Commons, Civil Engineering Commons, Computer Engineering Commons, Electrical and Electronics Commons, Metallurgy Commons, Ocean Engineering Commons, and the Structural Engineering Commons

See next page for additional authors

Recommended Citation
Parikin, Parikin; Dani, Mohammad; Iskandar, Riza; Jahja, Aziz Khan; Insani, Andon; and Mayer, Joachim (2019) "Comprehensive Inspection on the Experimental Ferritic Stainless Steel by Means of Transmission Electron Microscopy and Neutron Diffraction Techniques," *Makara Journal of Technology*: Vol. 23: Iss. 3, Article 1.
DOI: 10.7454/mst.v23i3.3746
Available at: https://scholarhub.ui.ac.id/mjt/vol23/iss3/1

This Article is brought to you for free and open access by the Universitas Indonesia at UI Scholars Hub. It has been accepted for inclusion in Makara Journal of Technology by an authorized editor of UI Scholars Hub.

Comprehensive Inspection on the Experimental Ferritic Stainless Steel by Means of Transmission Electron Microscopy and Neutron Diffraction Techniques

Authors

Parikin Parikin, Mohammad Dani, Riza Iskandar, Aziz Khan Jahja, Andon Insani, and Joachim Mayer

This article is available in Makara Journal of Technology: https://scholarhub.ui.ac.id/mjt/vol23/iss3/1

Makara J. Technol. 23/3 (2019), 103–110
doi: 10.7454/mst.v20i3.3746

Comprehensive Inspection on the Experimental Ferritic Stainless Steel by Means of Transmission Electron Microscopy and Neutron Diffraction Techniques

Parikin[1*], Mohammad Dani[1], Riza Iskandar[2], Aziz Khan Jahja[1], Andon Insani[1], and Joachim Mayer[2]

1. Science and Technology of Advanced Materials, National Nuclear Energy Agency (BATAN), South Tangerang 15314, Indonesia
2. Central Facility for Electron Microscopy (GFE), RWTH Aachen University, Ahornstrasse.55, D-52074 Aachen, Germany

[*]*e-mail: farihin@batan.go.id*

Abstract

The field of physical metallurgy is one of the primary beacons that guide alloy developments for multipurpose materials such as the in-core structure materials for pressure vessel components and heat exchangers. The surface microstructure of new ferritic steel with significant local constituent materials was characterized by high resolution powder neutron diffractometer (HRPD) and transmission electron microscope (TEM), combined with the energy dispersive X-ray spectroscopy (EDX). The alloy contains73% Fe, 24% Cr, 2% Si, 0.8% Mn, and 0.1% Ni, in %wt. The charge materials were melted by the casting techniques. The neutron diffractograms obtained shows five dominant diffraction peaks at (110), (200), (211), and (220) reflection planes, which is a typical structure for a body centered tetragonal system. The pattern also included some unidentified peaks which were verified to be $Al_2O_3.54SiO_2$, $Cr_{23}C_6$, and SiC crystals. A piece of alloy which taken from the middle of the ferritic ingots was also characterized by the HRPD; no unidentified peaks were observed. Results from the scanning transmission electron microscopy (STEM) combined with EDX analyses confirmed the neutron identified phase distributions. Also, oxides and carbides were observed to form mainly close to the surface of the steel. Cracks and pores which probably formed during the preparations were also identified close to the surface. Although the ferritic steel was successfully synthesized and characterized, some unidentified phases and defects could still be found in the produced ingots.

Abstract

Inspeksi Komprehensif pada Baja Feritik Eksperimental dengan Mikroskop Elektron Transmisi dan Teknik Difraksi Neutron. Bidang metalurgi fisik adalah salah satu suar primer yang memandu pengembangan paduan pada material serba guna, yaitu material struktur inti untuk komponen bejana tekan dan penukar panas. Struktur mikro permukaan baja feritik baru dengan kandungan lokal yang signifikan telah dikarakterisasi secara komprehensif dengan menggunakan difraktometer neutron serbuk resolusi tinggi (HRPD) dan mikroskop elektron transmisi (TEM) yang dikombinasikan dengan spektroskopi dispersif energi sinar-X (EDX). Paduan mengandung 73% Fe24% Cr2% Si0.8% Mn0.1% Ni dalam% wt. dicairkan dengan teknik casting. Difraksi neutron menampilkan lima puncak difraksi dominan pada bidang refleksi (110), (200), (211) dan (220), yang merupakan struktur tipikal untuk sistem tetragonal berpusat badan (*bct*). Pola difraksi menampilkan juga beberapa puncak yang tidak diharapkan; terdiri dari kristal: $Al_2O_3.54SiO_2$, $Cr_{23}C_6$ dan SiC. Sementara sampel paduan yang diambil di tengah bahan ingot feritik juga difraksi neutron dan tidak menampakkan puncak yang tidak diharapkan. Hasil lebih lanjut dari pemindaian mikroskop elektron transmisi (STEM) yang dikombinasikan dengan analisis EDX mengkonfirmasi distribusi fase yang teridentifikasi pada difraksi neutron. Selain itu, oksida dan karbida yang terbentuk dekat dengan permukaan bersama dengan retakan dan pori-pori, mungkin terbentuk selama proses preparasi. Meskipun, baja feritik telah berhasil disintesis, beberapa fase dan cacat yang tidak teridentifikasi masih dapat ditemukan dalam ingot yang diproduksi.

Keywords: 73Fe24Cr2Si0.8Mn0.1Ni ferritic steel, HRPD, STEM, EDX

1. Introduction

The ability to improve the performance of nuclear reactors as regards safety, proliferation resistance, economic performance, and minimization of waste, has been considerably defined by the advanced nuclear system. This improvement is the goal of the sixt h advanced generation IV-reactor concepts [1].

The structures of the materials used for the reactor components, most of which are metal alloys such as steels, are of great concern. A number of improved alloy compositions, both Ferritic-Martensitic (F/M) and Austenitic steels have been developed and are also continuously being developed. Corrosion is one of the major problems encountered by components operating in high-temperature environments. High-temperature corrosion is of great concern in energy production, engines, and industrial processes. It limits the life span of installations, restricts the utilization of the fuel, and disrupts the development of more economical environmentally sustainable processes and systems. Several areas of application, including combustion and gasification of biomass and waste, metallic materials for solid oxide fuel cells, and materials for industrial processes have become up-to-date issues.

Graphites and carbon-based ceramic composites are usually composed of the primary in-core structures, including of 2.25% Cr bainitic steel or 9% Cr martensitic steel for reactor pressure vessel, cross vessel component, and intermediate heat exchangers [2] which diverts heat from the primary side of the reactor to a hydrogen production plant. Such components place great demands on their construction materials. Therefore, high mechanical strength, creep resistance, and corrosion resistance are required to improve the life span by about 20 years.

Recently, improving nickel-based alloys for high-temperature applications was found to be beneficial [1], however, they are limited by the type of applications, optimum design, and quality of the minerals. Therefore, the new type of ferritic steel needs to be promoted and synthesized for self-conditional needs.

As regards the advanced reactor materials research program, scientists of the Indonesian National Nuclear Energy Agency (BATAN) have successfully synthesized ferritic super alloy steel using local raw materials. The alloy contains 73% Fe, 24% Cr, 2% Si, 0.8% Mn, and 0.1% Ni, in %wt. This ferritic steel [3] was proposed to be useful as structural components for multi-purpose facilities (i.e., reactor structural materials). Therefore, the material must have high mechanical strength, high operating temperature, high corrosion resistance, and irradiation, especially neutron scattered from the reactor. These are the main desired properties for the synthesized steels for the reactor application.

The ferritic steel has been reported to have the super alloy phenomenon as regards its corrosion resistance [4], hardness, and tensile-impact strengths [5]. The main objective of synthesizing the new ferritic alloys is to significantly improve the corrosion resistance. To achieve this objective, alloy with reduced nickel and high chromium contents is desired. The alloy steel is also expected to have such advantages as high operating temperature, ease of fabrication, and economic competitiveness, hence, good for structural applications in the reactor and as well, for general applications. To produce a ferritic alloy with low carbon content, non-standard chemical composition was synthesized, on a laboratory scale, by casting method [6]. Considering the Cr content of the alloy, the steel was expected to have superior properties over the T91 and T92 alloys, therefore, good candidate material for structural applications in the nuclear reactor [7].

The main aim of this research is to understand the mechanism behind their high mechanical properties, high-temperature operation, and high corrosion resistance of the high-temperature material. These properties are desired for applications as in structural components of the reactor. The relationship between the properties and performance of the materials can be traced to the microstructures. Therefore, microstructural observation of the synthesized materials is the main objective of this research.

2. Experimental

A standard laboratory steel casting was carried out. The composition of the alloy was first computed after which the constituents were weighed using the precision balance. The appropriate amount of the base materials weighed was melted in an electromagnetic induction furnace. The ferritic super alloy was synthesized from granular ferro-scrap, chromium steel scrap, plain carbon steel scrap, FeSi75, low carbon FeCr65, pure nickel, FeMn, slag remover, and pure aluminum which were melted in the furnace. The processes, from preparation to the casting, remained the same for the ferritic steel, and other synthesized steel. The compositions synthesized alloy is shown in Table 1.

Aluminum was added to enhance degassing during casting. The adopted process of casting followed the procedure for commercial production. The obtained ingots were formed into bulk samples by simple metal forming procedural standards after which they were finished by cutting and rolling processes. Besides the produced steel, the significance of the metal forming process used [8] may be justified by its overall cost-effectiveness due to the low material and energy consumption of the sheet-forming process. The elemental compositions of the samples (dimension 1.0 x 3.5 x 15 cm^3) were obtained by the Optical Emission Spectrometry (OES); the mean result is presented in Table 1.

Table 1. The Chemical Composition of the Ferritic Steel

Element	%wt.
Fe	72.97
Ni	0.12
Cr	23.71
Mn	0.82
Si	2.02
Al	0.01
Ti	0.01
Sn	0.01
Nb	0.01
C	0.26
S	0.01
P	0.02
V	0.06

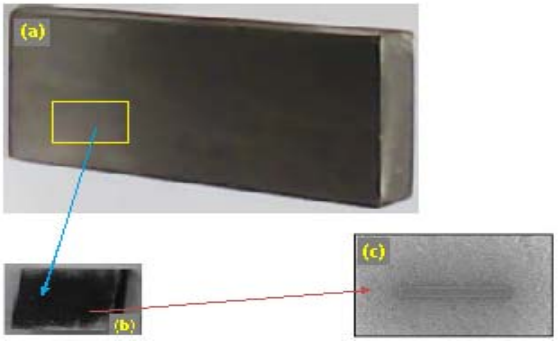

Figure 1. Photographs of the Ferritic Steel Sample; (a) A 15.0 x 3.5 x 1.0 cm^3 As-cast Sample (b) A 3.0 x 2.0 x 1.0 mm^3 Prior to Polishing-Thinning and (c) Deposition of Protective Layer on Area where Focused Ion Beam (FIB) Lamella was Prepared

Figure 1 shows photographs of the prepared sample. The test samples were in the form of base metal of ferritic steel with dimensions as in (a) for the OES tests and neutron diffraction experiments, and (b-c) for TEM observations. The crystal structures of the samples were obtained using the neutron diffractometer and then refined by the Rietveld method. The HRPD has 32 highly sensitive detectors that can simultaneously measure the diffraction patterns of a sample. Since it utilizes neutrons that have higher penetrating power than X-rays by some order, it would be more sensitive due to the interaction of the with the atomic nuclei, hence, small amounts of other crystals remaining in the formation of materials can be detected in more detail than in the X-rays. The device is, therefore, an excellent non-destructive tool for characterizing material's crystal structures. The neutron diffraction method is the preferred technique for measuring rotated bulk structures in most engineering materials. A thermal neutron beam scattered from the reactor allows some to deeply analyze the structure of a thick material by a simple preparation. A complete set of experimental data would, therefore, be obtained by this technique.

A more detailed analysis of the surface microstructure was carried out using the TEM. A standard procedure for sample preparations for TEM analysis was carried out using the FIB technique. In this case, the "in-situ lift-out technique" was applied, whereas, an electron transparent sample was prepared using the FIB techniques on FEI Strata 205 single beam instruments (see Figure 1c). The lamella was investigated on a Schottky field emission Zeiss Libra 200 FE transmission electron microscope operated in scanning mode at 200 kV. The microscope has an in-built column corrected filter and is equipped with a high angle annular dark field and X-flash energy dispersive spectroscopy (EDX) detectors from Fischione and Bruker respectively. The EDX data was analyzed with the help of the ESPRIT software from Bruker, where the mapping features were used as complementary information to identify the crystalline compounds that are left in the synthesized steel materials.

3. Results and Discussion

Diffraction Pattern. The result of the neutron diffraction measurements [9] of the steel samples is shown in Figure 2. A wavelength of 1.82 Å was used. There is an adequate peak to background ratio, hence, the actual diffraction peaks can be clearly distinguished from the background counts. The diffraction pattern is typically that of a body centered tetragonal (*bct*) [10] crystal system, which shows four principal diffraction peaks. The planes are diffracted at 2Θ-angle of 53.3°, 78.7°, 101.9°, and 127.5°, respectively and numerically grouped accordingly, alternating the odd and even numbers. The parts of diffraction peaks in the 2Θ-angle measurements ranging from 2.5°–147° are unidentified peaks that emerged from undesirable contaminants. These contaminants may hinder the structural refinements, due to the difficulty in achieving convergence of good calculations in processing the fitting data.

Table 2. Initial Structure Parameters of Ferritic "*Bct*–system" Steel

Sym.	S.G.	Lattice Parameters			Vol. (Å^3)	Num. of At.; Z	*x,y,z*
		$a = b$ (Å)	c (Å)	$\alpha = \beta = \gamma$ (°)			
Fe	I4 mmm	2.86	2.87	90	23.61	2	0,0,0

There is evidence of unidentified peaks in the range of the sample diffraction patterns. In the entire diffraction zone, the crystal shows a mixture of the total diffraction pattern of a crystal having a *bct* symmetry, and other phases shown by the reflections of some lower-intensity impurities.

A computer special application code, Rietveld Analysis (Reitan), was used to refine the diffraction pattern. The initial crystallographic parameters for the Rietveld refinement are listed in Table 2. The listed crystallographic data was used as the initial input data in the Rietveld refinement [11], [12]. The initial refinement was carried out using a single-phase model (a pseudo-Voight function which is a linear combination of Gaussian and Lorentzian functions), as listed in Table 2. The final fitting gave less satisfactory weighted-profile factor (R_{wp}) and reliability factor (S). The values obtained are quite high which could be due to the presence of some unidentified peaks. Meanwhile, successive peaks in the diffractogram in order of appearance are the (110), (200), (211), and (220) planes. The diffraction pattern is a mixture of the standard and unidentified peaks which could enhance the background counts.

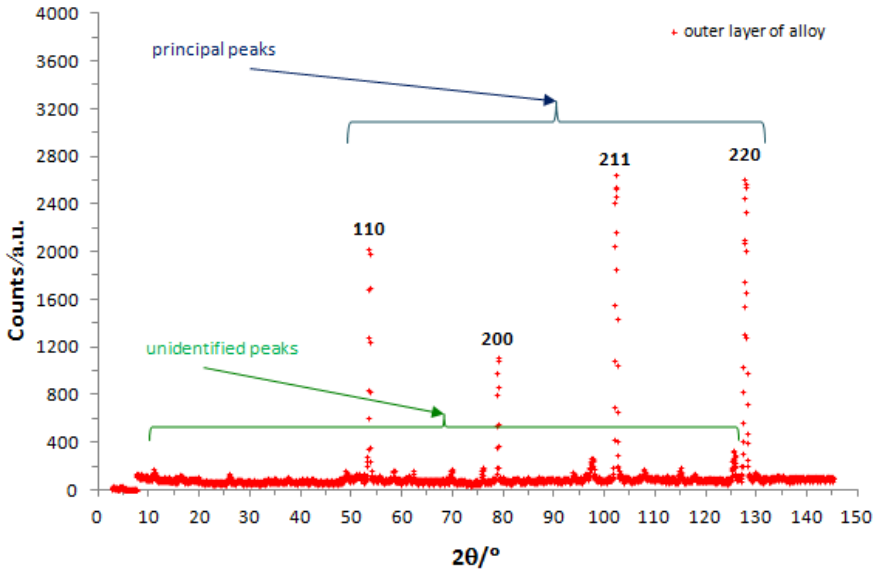

Figure 2. High Resolution Powder Neutron Diffractometer (HRPD) Pattern of Ferritic Steel Sample Using 1.82 Å in Wavelength

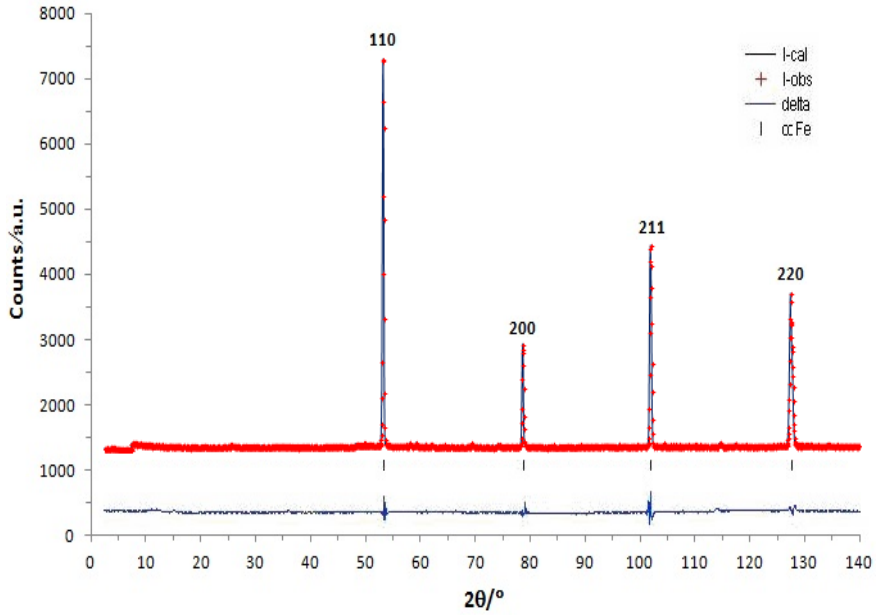

Figure 3. Refinement Pattern of Ferritic Steel "Free Defects" Sample from HRPD-1.82 Å

Figure 3 shows the diffraction pattern for the "free defect" sample for a single-phase Rietveld refinement of the steel, whereas, Figure 2 shows the pattern for the neutron diffraction measurements of the ferritic steel. The overall profile of the material shows that the material is devoid of impurities. Rietveld refinements [13]-[15] yielded a quite satisfactory fitsfactor value, attaining the weighted-profile *R*-factor R_{wp} value of 8.1 %, and reliability factor *S* of 1.2. The residual profile seems to be a straight line with a minuscule ripple at each peak position. Signs for line broadening were observed; some vertical lines under standard patterns and models. The lines indicate the principal peak position of the ferritic phase in steel samples. The full pattern of the standard profile and refinement is shown in the diagram. The results clearly show that the crystalline symmetry belongs to the body centered tetragonal (*bct*) crystal system. As shown in the figure, the reflection planes of (110), (200), (211), and (220) are patterned alternating even and odd numbers.

Peak Identification. The diffraction pattern also shows that in addition to the primary peaks of the *bct* structure, there are some unidentifiable peaks. Based on the result of Rietveld refinements, the goodness of fits factor (R_{wp}:*S*) is not quite satisfactory. These peaks can be manually identified by evaluating the d_{hkl} spacings. The d_{hkl} was calculated using the Bragg formula; $\lambda = 2\, d_{hkl} \sin \Theta$. The correlation between $(1/d_{hkl})$ and $(2\sin\Theta/\lambda)$ was determined by the least square (LS) method [16], [17]. Figure 4 shows the calibration curve of the JCPDS data between 2Θ and d_{hkl} obtained by the LS-method.

The crystallographic data following the 2Θ and d_{hkl} of Al_2O_3.54 SiO_2 (44–0003), $Cr_{23}C_6$ (35–0783) and SiC (42–1360) were taken from the JCPDS database [18] to verify the linear equations of $x = (2\sin\Theta/\lambda)$ versus $y = (1/d_{hkl})$. The *d*-spacings for the obtained diffraction angles were computed using the equations. Few of the calculated *d*-spacings of the unidentified peaks conforming to the JCPDS data are listed in Table 3.

Some of the computed *d*-spacings overlapped with one-another following a continuous line, starting from aluminum silicate, through chromium carbide, and silicon carbide. It was found that two phases, $Cr_{23}C_6$, and SiC, have a fairly strong linear correlation with the χ-square (R^2) values exactly at unity (1). However, it is very understandable for the $Al_2O_3.54SiO_2$ phase to have the value of R^2 close to unity (0.99) in the LS-curve calibrations. In the table, it is observed that the first three planes belonging to the $Al_2O_3.54SiO_2$ phase have slightly wider *d*-spacing values between the LS and the JCPDS data. Also, the phase is observed to have a complex length crystal structure, which indicates a combination of SiO_2 and Al_2O_3 crystals.

Microstructural Observation. Figure 5 shows an image of the sample area where the FIB lamella was prepared (marked by the rectangle). The sample surface contains coagulations, pores, and cracks which is probably due to non-uniform heating or cooling (rapid heating or cooling) during the heat treatment process.

STEM angular dark field (ADF) image [19] revealed a more detailed condition of the sample. The dark regions on the surface of the sample, as shown in Figure 5, suggest that pores or oxides were formed as secondary phases. Some differences in the contrast were also detected on the area close to the surface which infers that some defects formed along the lamella. These defects may have been induced by machining processes. These defects were also observed in previous reports for a similar sample [20] and for austenitic sample [21].

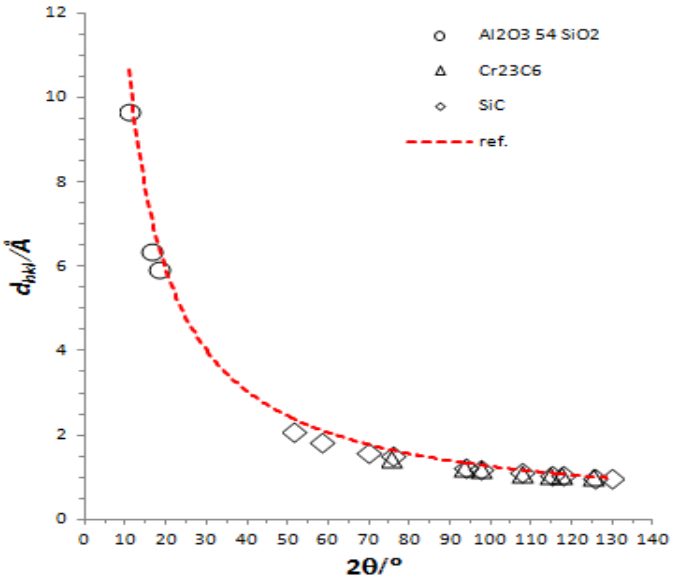

Figure 4. Calibration Curve to Identify d_{hkl} of $Al_2O_354SiO_2$, $Cr_{23}C_6$, and SiC in the Ferritic Steel Sample

Table 3. Peak Identification via Comparation of d-spacings between the JCPDS Database and Unidentified Peaks

Compounds		$Al_2O_354SiO_2$	$C_{23}C_6$	SiC
2θ (°)		10.88	75.70	51.38
		16.20	93.60	58.14
		18.10	97.38	69.52
			107.57	75.70
			114.68	93.60
			117.38	97.38
			125.35	107.57
				114.68
				117.38
				125.35
				129.52
Plane; *hkl*		1 1 1	6 4 0	0 0 6
		3 0 1	8 2 2	0 0 7
		0 3 1	6 6 2	1 0 19
			9 3 1	1 1 0
			8 4 4	0 0 10
			7 7 1	2 0 2
			10 2 2	1 0 10
				2 0 6
				2 0 7
				1 0 34
				2 1 0
Relative Intensity; *I* (a.u.)		17	<1	10
		11	12	20
		5	15	10
			1	90
			6	40
			3	10
			1	20
				40
				10
				10
				50
	Least Square Calibration	9.71	1.48	2.09
		6.37	1.25	1.86
		5.95	1.22	1.60
			1.12	1.54
			1.08	1.25
			1.06	1.20
			1.02	1.13
				1.09
				1.06
				1.01
				1.00
***d*-spacing (Å)**	**Reference (JCPDS)**	9.68	1.48	2.09
		6.34	1.25	1.87
		5.92	1.21	1.59
			1.11	1.48
			1.09	1.24
			1.07	1.20
			1.02	1.13
				1.08
				1.06
				1.02
				1.00

Figure 5 shows the TEM image of about 3.5 μm cross-section depth (transverse direction) from the surface of the ferritic super alloy steel sample. Pores and cracks (defects) are observed on the surface. As shown in the image the pores extend to about 3 μm depth, close to the real surface of the steel. In the figure, the thickness mass contrast, which is responsible for the density cannot be differentiated. The more dominant elemental contrast is observed where oxides (alumina or SiO) are darker than the matrix. The smooth gray color below 3.5 μm depth shows the "free defects" parts of the compact steel. The compaction of materials can be clearly traced from the upper surface down to beyond the real surface via the gray color degradation. The alumina interface is crystalline according to the HRTEM data. The pores indicate the thin layer of SiO_2 formed on the matrix-alumina interface (see Figure 7a for the Al, Si, and O frames.) The silicon carbide (on the top right) is indicated by the amorphous regions or nanocrystalline. A previous investigation by Dani *et al.* [22] revealed that the precipitations indicate the presence of the $(Cr, Fe)_7C_3$ carbide. Precipitates mainly form within the dendrite matrix and the dendrite boundaries. The presence of the precipitates at the dendritic boundaries does not lead to Cr deflection zones. Therefore, it is inferred that the presence of the precipitates can improve the mechanical properties of this new type of Ferritic Stainless Steel.

The part of the sample close to the surface contains significant cracks and pores which make the outer part of the sample less dense than in inner part. The outer part of the material is less compacted than the inner part due to the presence of these pores and cracks formed at the surface of the steel. Consequently, mechanical treatments are recommended to remove the less compacted layers from the material by machining (cut-roll) process. This machining should be done until the compact layer is reached if the steel is to be applied as multipurpose structural components.

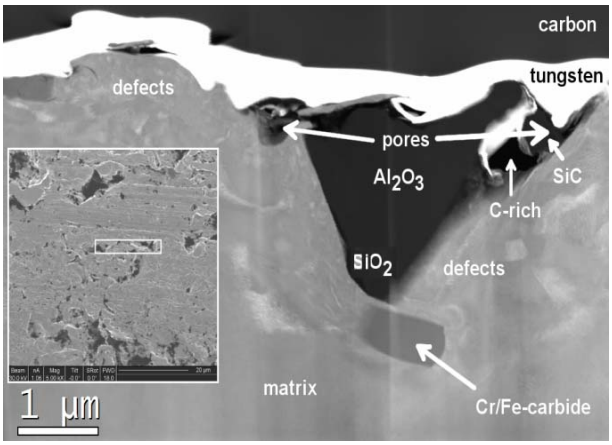

Figure 5. STEM with Angular Dark Field (ADF) Image Taken from the Area Up to 3.5 μM of the Ferritic Steel Sample Surface. The Insert is FIB-Secondary Ion Image on the Surface of the Ferritic Steel Sample where the Lamella was Prepared

Elemental Spectroscopy. Elemental analysis at higher magnification was performed using the STEM-EDX techniques. Figure 6a shows the elemental maps taken from the area shown in Figure 5. The black areas in the figures show the presence of oxygen which indicates the formation of oxides, presumably alumina, or silica in the areas. Based on the EDX analysis, in addition to these oxides, carbides (possibly chromium carbide) were also formed close to the alumina oxide grain. There was no indication of the formation of chromium oxide in the sample. However, large grains of aluminum oxide was formed. Silicon oxide also formed at the interface between the matrix and the aluminum oxide.

Another lamella cut from another part of the sample devoid of pores formed at the surface as shown in Figure 6b. However, micropores and cracks were observed in the sample. Some oxygen enrichments were also detected along the cracks which could further trigger the formation of intergranular cracks. These intergranular cracks may slowly-migrate to and may move fast along the grain boundaries. It can be also seen from the STEM-ADF image that the crack formed in one direction which is attributed to the machining processes. The carbon elemental map also shows a carbon-rich area formed at the dark area which probably contains amorphous carbon.

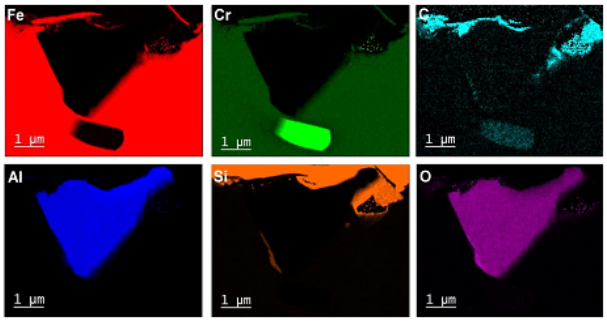

(a)

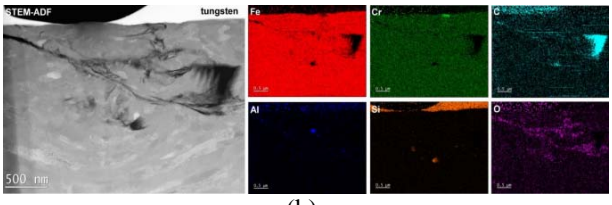

(b)

Figure 6. (a) STEM-ADF EDX Elemental Maps of Areas with Pores and Defects Formed at the Upper Part of the Lamella. Higher Signals of Aluminum and Silicon on Cracks and Pores Suggest that this Area Contains Probably Alumina and Silicon Oxides. Please Note that the Silicon Signal at the Top of the Sample is an Artifact Caused by the Tungsten Signal which Overlaps with the Silicon. (b) STEM-ADF and EDX Elemental Maps from another FIB Lamella Prepared from the Pore-Free Ferritic Steel Sample Surface. Micropores and Microcracks can be Still Found in this Area

4. Conclusions

A successful synthesis of new Ferritic Stainless Steel from local materials is reported. The alloy was formed by casting techniques and finished by machining processes. The neutron diffraction shows some unidentified peaks, in addition to the principal ferritic steel profile, which belongs to impurity compounds formed in the material. These impurities were verified to be small amounts of $Al_2O_354SiO_2$, $Cr_{23}C_6$, and SiC crystals. For comparison, other pieces of samples of the alloy taken from the middle of ingots were also characterized by the neutron diffractometry. The pattern obtained is free from undesirable crystals. Further STEM-EDX analysis confirmed that those secondary phases, mainly cracks, pores, and oxides, were found at 3 µm below the surface of the sample. The secondary phases and defects may have been induced during the preparation processes. Mechanical treatments are, however, recommended to scrape off the less compacted layers of about 3.5 µm in thickness for the sustainability of the structural component fabrications.

Acknowledgements

The authors would like to express their gratitude to Head of PSTBM and BSBM, Mr. Agus Hadi Ismoyo, Mr. Imam Wahyono, Mr. Bambang Sugeng, Mr. Rohmad Salam and Mr. Heri Mugihardjo for their kindness and helps. This work has been carried out in parts with GFE–RWTH–Aachen Germany of TEM Analysis. Financial support of DIPA 2016–2017 is also gratefully acknowledged.

References

[1] NEA-OECD, Status Report on Structural Materials for Advanced Nuclear Systems, Nuclear Energy Agency Organisation for Economic Co-operation and Development, OECD, NEA No.6409, 2013.
[2] E. Taban, E. Kaluc, T. Atici *et al.*, 9–12% Cr Steels: Properties and Weldability Aspects, The Situation in Turkish Industry, Proc. 2nd Int. Conf. on Welding Tech. and Exhibition, 2012, p. 203.
[3] N. Effendi, T. Darwinto, A.H. Ismoyo, Parikin, Indonesian J. Mat. Sci. 15/4 (2014) 187.
[4] Parikin, B. Sugeng, M. Dani, S.G. Sukaryo, Indonesian J. of Mat. Sci. 18/4 (2017) 179.
[5] A.H. Ismoyo, Parikin, Mechanical Testing on the 73Fe24Cr2Si0.8Mn0.1Ni Ferritic Steel for Structural Materials, submitted to Indonesian J. Mat. Sci., 2018.
[6] P.J.G. Nieto, V.M.G. Suárez, J.C.A. Antón *et al.*, Mater. 8 (2015) 3562.
[7] J.P. Zou, K. Shimizu, Q.Z. Cai, J. Iron Steel Res. Int. 22/11 (2015) 1049.
[8] S. Wagner, M. Sathe, O. Schenk, Int. J. Adv. Man. Tech. 71/5–8 (2014) 973.

[9] T.M. Holden, Y. Traore, J. James, J. Kelleher, P.J. Bouchard, J. Appl. Cryst. 48/2 (2015) 582.
[10] V.M. Gundyrev, V.I. Zel'dovich, Phys. Met. Metallogr. 115/10 (2014) 973.
[11] Parikin, A.H. Ismoyo, A. Dimyati, Makara J. Tech. 21/2 (2017) 49.
[12] V. Kumar, S. Kumari, P. Kumar, M. Kar, L. Kumar, Adv. Mater. Lett. 6/2 (2015) 139.
[13] B. Cai, B. Liu, S. Kabra, Y. Wang, K. Yan, P.D. Lee, Y. Liu, Acta Mater. 127 (2017) 471.
[14] O. Rivin, A. Broide, S. Maskova *et al*., Hyperfine Interact. 231 (2015) 29.
[15] A.A. Saleh, D.W. Brown. E.V. Pereloma, B. Clausen, C.H.J. Davies, C.N. Tomé *et al*., Appl. Phys. Lett. 106/17 (2015) 1911.
[16] J.B. Wiskel, L. Junfang, O. Omotoso, D.G. Ivey, Metals 6/4 (2016) 90.
[17] M. Frentrup, L.Y. Lee, S.L. Sahonta, M.J. Kappers, F. Massabuau, P. Gupta *et al*., J. Phys. D: Appl. Phys. 50 (2017) 1.
[18] I. Bruno, S. Gražulis, J.R. Helliwell, S.N. Kabekkodu, B. McMahon, J. Westbrook, Data Sci. J. 16 (2017) 38.
[19] Parikin, M. Dani, A.K. Jahja, R. Iskandar, J. Mayer, Int. J. Tech. 9/1 (2018) 78.
[20] M. Dani, Parikin, R. Iskandar, A. Dimyati, Indones. J. Sci. Mat. 18/4 (2017) 173.
[21] M. Dani, Parikin, A. Dimyati, A.K. Rivai, R. Iskandar, Int. J. Tech. 9/1 (2018) 89.
[22] M. Dani, A. Dimyati, Parikin, F. Rohman, R. Iskandar, A.K. Jahja *et al*., Malay. J. Fund. Appl. Sci. 15/6 (2019) 831.